Editors' choice

Skull of a dromaeosaurid dinosaur *Shri devi* from the Upper Cretaceous of the Gobi Desert suggests convergence to the North American forms

ŁUKASZ CZEPIŃSKI

Czepiński, Ł. 2023. Skull of a dromaeosaurid dinosaur *Shri devi* from the Upper Cretaceous of the Gobi Desert suggests convergence to the North American forms. *Acta Palaeontologica Polonica* 68 (2): 227–243.

Numerous dromaeosaurid taxa recovered from the Upper Cretaceous strata of the Gobi Desert raise questions over niche partitioning among closely related species. Here, I describe a dromaeosaurid specimen from the Baruungoyot strata of the Khulsan locality, containing a partial skull in close association with the left hind limb. The material can be referred to the velociraptorine *Shri devi*, until now known only from a single specimen lacking a skull, collected from the same site. The referral is based on the apomorphic morphology of the pes, including the highly hypertrophic ungual of the second digit and details of the metatarsus. The skull of *S. devi* confirms its close affinities with *Velociraptor mongoliensis*, but shows distinctive features among Velociraptorinae, including a short antorbital fenestra, a Z-shaped maxillo-jugular suture, a distinct labial ridge above the supralabial foramina row of the maxilla, and the posterior position of the last maxillary tooth. The skull of *S. devi* is slender, but relatively short when compared to other velociraptorines, suggesting convergence to the North American eudromaeosaurians. The Baruungoyot strata with *S. devi* represent less arid conditions than the aeolian Djadokhta strata yielding *V. mongoliensis*, supporting earlier observations linking the elongation of the dromaeosaurid snout with the environment.

Key words: Dinosauria, Theropoda, Dromaeosauridae, convergence, Cretaceous, Mongolia, Gobi Desert.

Łukasz Czepiński [lczepinski@twarda.pan.pl; ORCID: https://orcid.org/0000-0002-8621-3888], Institute of Palaeobiology, Polish Academy of Sciences, ul. Twarda 51/55, 00-818 Warsaw, Poland; Institute of Evolutionary Biology, Faculty of Biology, Biological and Chemical Research Centre, University of Warsaw, ul. Żwirki i Wigury 101, 02-089 Warsaw, Poland.

Received 3 March 2023, accepted 30 May 2023, available online 21 June 2023.

Introduction

Dromaeosauridae is a group of small to medium-sized carnivorous theropod dinosaurs known mainly from the Cretaceous of Asia, North and South America, and Europe (Turner et al. 2012; Pittman et al. 2020b). They are characterized by, among all, a hypertrophied claw on the pedal digit II, and tightly interlocked caudal vertebrae bound by elongated prezygapophyses; most of them were also probably covered in feathers (Turner et al. 2012; Pittman et al. 2020a).

The fossil record of this group is often fragmentary, and only a few species were described based on more than isolated bones (Pittman et al. 2020b). One of the exceptions is *Velociraptor mongoliensis* Osborn, 1924, known from several quite complete specimens collected from the Upper Cretaceous sediments of the Djadokhta strata of the Gobi Desert, including both cranial and postcranial remains (Sues 1977; Barsbold 1983; Norell and Makovicky 1997, 1999; Barsbold and Osmólska 1999; Norell et al. 2004; Hone et al. 2012).

Recent years led to the recognition of a number of new dromaeosaurid taxa from the Upper Cretaceous strata of the Gobi Desert (Figs. 1, 2; SOM: table S1, Supplementary Online Material available at http://app.pan.pl/SOM/app68-Czepinski_SOM.pdf), including the newly recognized group Halszkaraptorinae (Osmólska 1982; Turner et al. 2007; Cau et al. 2017; Cau and Madzia 2018; Lee et al. 2022), and members of Velociraptorinae (taxa closely related to *V. mongoliensis*) such as *Adasaurus mongoliensis* Barsbold, 1983, *Tsaagan mangas* Norell, Clark, Turner, Makovicky, Barsbold, and Rowe, 2006, "*Velociraptor*" *osmolskae* Godefroit, Currie, Li, Shang, and Dong, 2008, *Linheraptor exquisitus* Xu, Choinere, Pittman, Tan, Xiao, Li, Tan, Clark, Norell, Hone, and Sullivan, 2010, *Shri devi* Turner, Montanari, and Norell, 2021, and *Kuru kulla* Napoli,

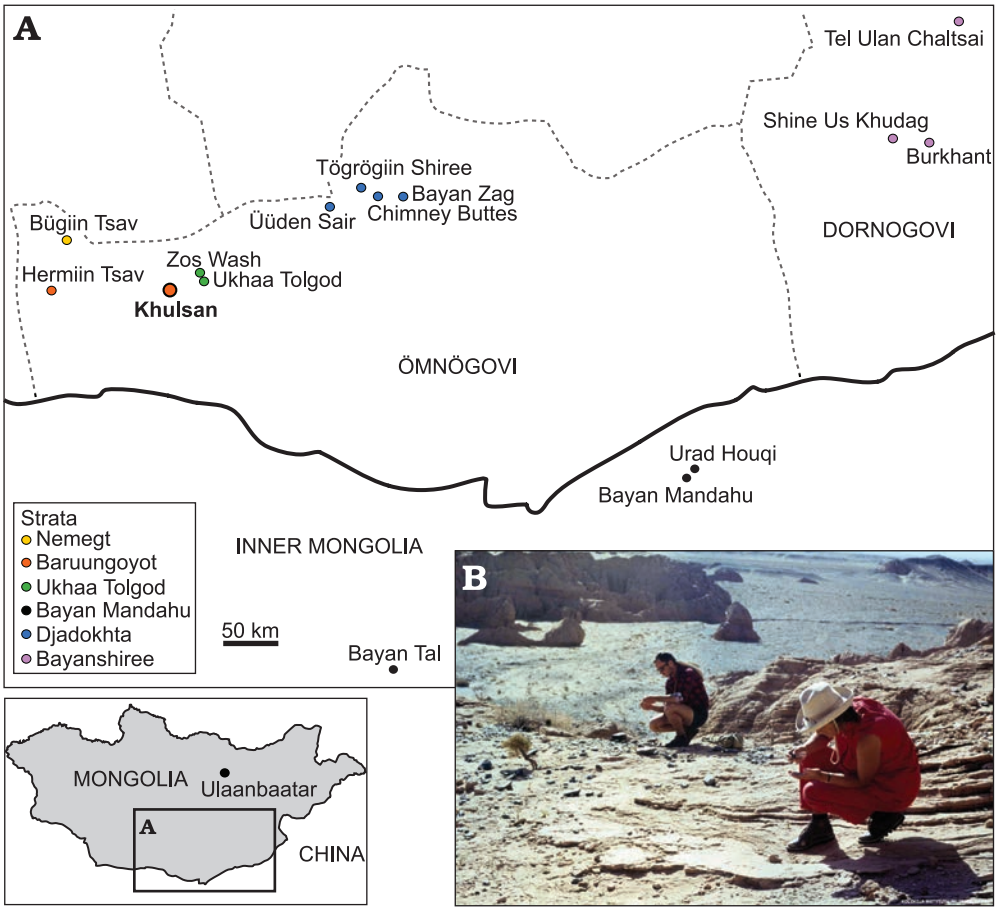

Fig. 1. **A**. Map of Mongolia and Inner Mongolia of China with the Upper Cretaceous sites yielding remains of dromaeosaurid dinosaurs. **B**. Photograph of Khulsan locality, from where the specimen described in this paper was collected, photographed in the 1970 during the Polish-Mongolian Paleontological Expeditions (from the Collections of the Institute of Palaeobiology PAS). Geographic data from: Jerzykiewicz and Russell 1991; Jerzykiewicz et al. 1993; Norell and Makovicky 1999; Dingus et al. 2008; Godefroit et al. 2008; Watabe et al. 2010; Tsogtbaatar et al. 2019; Chen et al. 2022. Map modified from Czepiński 2020b. Transcriptions of the locality names follow Benton (2000).

Ruebenstahl, Bhullar, Turner, and Norell, 2021, nearly all of which are represented solely by type specimens.

Here I describe cranial and postcranial dromaeosaurid material from the Khulsan site of the Upper Cretaceous Baruungoyot strata in the Gobi Desert. The specimen includes the articulated pes, which makes it possible to compare and refer to the *Shri devi* holotype collected from the same locality. It supplements the original description of this species, as the holotype lacks the cranium and provides evidence for a relatively short skull within Velociraptorinae, convergent to the North American dromaeosaurids.

Institutional abbreviations.—AMNH FARB, American Museum of Natural History, Fossil Amphibians, Reptiles, and Birds, New York, USA; IMM, Inner Mongolia Museum, Hohhot, China; IVPP, Institute of Vertebrate Palaeontology and Paleoanthropology, Chinese Academy of Sciences, Beijing, China; MPC, Institute of Paleontology, Mongolian Academy of Sciences, Ulaanbaatar, Mongolia; PIN, Palaeontological Institute, Russian Academy of Sciences, Moscow, Russia; ROM, Royal Ontario Museum, Toronto, Canada; SMP, State Museum of Pennsylvania, Harrisburg, Pennsylvania, USA; TMP, Royal Tyrrell Museum of Palaeontology, Drumheller, Alberta, Canada; UALVP, University of Alberta Laboratory for Vertebrate Palaeontology; Edmonton, Alberta, Canada; YPM, Yale Peabody Museum of Natural History, New Haven, Connecticut, USA; ZPAL, Institute of Paleobiology, Polish Academy of Sciences, Warsaw, Poland.

Material and methods

The cranial elements of the ZPAL MgD-I/97 were scanned using the Nikon/Metris XT H 225 ST scanner housed at the Military University of Technology, Warsaw, Poland, with a voltage of 170 kV, current of 37 μA, and the voxel size equal 200 μm. Three-dimensional models of the postcranial elements of the ZPAL MgD-I/97 were prepared using the Shining 3D EinScan Pro 2X 3D scanner and EXScan Pro 3.2.0.2 software. The number of turntable steps was varied and chosen depending on the specimen. The volume data from the CT were later processed using Fiji software (Schindelin et al. 2012) and then the 3D-model was generated using Drishti 2.7 (Limaye 2012). The framework for

the 3D visualization of the CT scan followed Semple et al. (2019). The obtained models from the CT and surface scans were later processed in Meshlab 2020.12 software (Cignoni et al. 2008) using the Lattice and Radiance Scaling shaders. The meshes of the cranial material are available at the Morphosource (https://www.morphosource.org/concern/biological_specimens/000524422).

The principal component analysis (PCA) was performed in the PAST software (Hammer et al. 2001). To remove the ontogenetic factor, the measurements of the cranial material were scaled to the antorbital fenestra length, while the pedal elements were scaled to the length of the phalanx III-1. PCA was performed using the variance–covariance matrix, with the missing values estimated or filled by the iterative imputation method.

The phylogenetic analyses were performed in TNT v. 1.6 (Goloboff and Morales 2023), using a "New Technology Search". The maximum number of trees was set to 10 000, with default parameters of the Random, Consensus and Exclusive Sectorial Search, and default parameters of the Ratchet, Drift and Tree Fusing.

Systematic palaeontology

Dinosauria Owen, 1842

Theropoda Marsh, 1881

Dromaeosauridae Matthew and Brown, 1922

Velociraptorinae Barsbold, 1983

Genus *Shri* Turner, Montanari, and Norell, 2021

Type species: *Shri devi* Turner, Montanari and Norell, 2021; Khulsan, Baruungoyot strata, Ömnögovi Province, Mongolia, Upper Cretaceous.

Shri devi Turner, Montanari and Norell, 2021

Figs. 2–4.

1981 *Velociraptor* sp. Osborn, 1924; Osmólska 1981: 88, table 2.
1982 *Velociraptor* sp. Osborn, 1924; Osmólska 1982: 445.
1999 *Velociraptor mongoliensis* Osborn, 1924; Barsbold and Osmólska 1999: 191, figs. 7A–F, 8.
1999 Dromaeosauridae indet. Matthew and Brown, 1922; Norell and Makovicky 1999: 3, fig. 24.
2007 *Velociraptor mongoliensis* Osborn, 1924; Feduccia et al. 2007: 376, fig. 2.
2021 Eudromaeosauria indet. Longrich and Currie, 2009; Napoli et al. 2021: 39.

Holotype: MPC-D 100/980, a partial articulated skeleton (including cervical, dorsal, and proximal caudal vertebrae, the right femur, the right and left tibiotarsa, and the right pes) lacking a skull (Turner et al. 2021).

Type locality: Khulsan, Ömnögovi Province, Gobi Desert, Mongolia.

Type horizon: Baruungoyot strata, ?Campanian, Upper Cretaceous (Jerzykiewicz and Russell 1991).

Material.—ZPAL MgD-I/97, a partial skull (including left jugal, left lacrimal, left maxilla, fragment of the right maxilla, palatine elements, both dentaries lacking the anterior-most portions, both splenials, surangulars, and angulars) in close association with a distal portion of the left hindlimb (containing the distal parts of the left fibula and tibia, astragalus and complete pes, with four metatarsals and all phalanges) from the type locality and horizon.

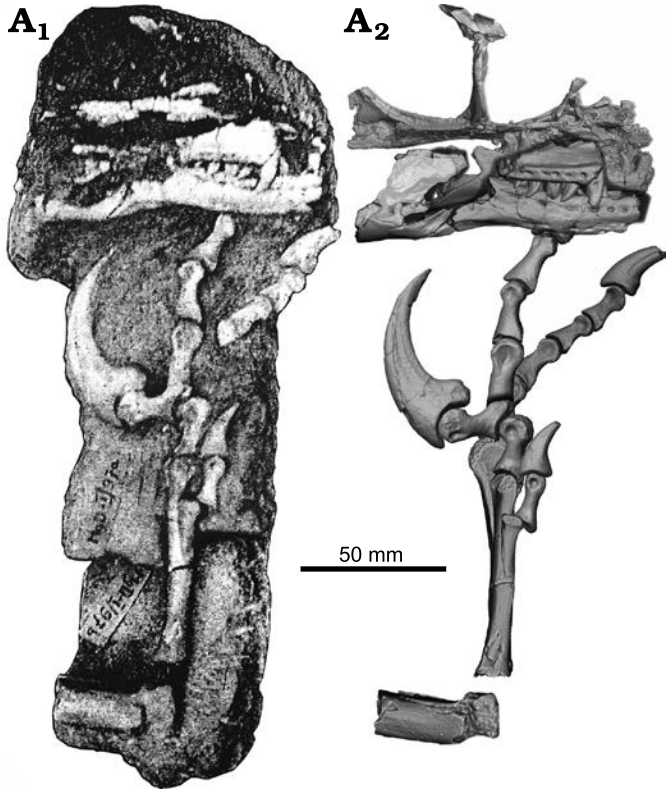

Fig. 2. Dromaeosaurid dinosaur *Shri devi* Turner, Montanari, and Norell, 2021 (ZPAL MgD-I/97) from the Upper Cretaceous, Khulsan, Ömnögovi, Gobi Desert, Mongolia. Specimen prior to the preparation work (A_1), and the 3D model of the skeleton, based on the CT and surface scanner data, with elements arranged as originally found (A_2).

Emended diagnosis.—Turner et al. (2021) diagnosed *Shri devi* on base of the following unique combination of features: large epipophyses on the first dorsal vertebra overhanging the posterior margin of the postzygapophysis (autapomorphy); two first dorsal vertebrae each with two dorsoventrally aligned pleurocoels on each side (autapomorphy); posteriorly inclined scar on the lateral surface of the neural arch (autapomorphy), a relatively long metatarsus (44% of the femur length), and proportionally long ungual phalanx on pedal digit II (101% to 104% of the metatarsal II length in MPC-D 100/980 and ZPAL MgD-I/97, respectively; modified after Turner et al. 2021).

Based on data derived from the new material, *S. devi* can be further diagnosed by: a short antorbital fenestra of subequal anteroposterior and dorsoventral axes with the ventral margin steeply inclined anterodorsally (shared with *Atrociraptor marshalli*, *Saurornitholestes langstoni*, and *Sinornithosaurus millenii*); a distinct longitudinal labial ridge determining the ventral margin of the antorbital fossa just above the supralabial foramina row, parallel to the alveolar margin of maxilla (shared with *Velociraptor mongoliensis* but more prominent

in *S. devi*); the last maxillary tooth positioned posterior to the anterior extremity of the maxillo-jugal suture (shared with *Atrociraptor marshalli* and *Saurornitholestes langstoni*); the Z-shaped suture between maxilla and jugal (shared with *Atrociraptor marshalli* and *Saurornitholestes langstoni*); the anteroventral process of quadratojugal projecting anterior to the posterior orbital margin of the jugal (autapomorphy); a short posterodorsal process of the lacrimal (autapomorphy); weakly developed, laterally positioned longitudinal tubercles on the anterior surfaces of metatarsals II and III (shared with *Linheraptor exquisitus*).

Description.—ZPAL MgD-I/97 represents a medium-sized individual of a velociraptorine dromaeosaurid. The partial skull is closely associated with a left pes, such that the ungual of the fourth digit is below the lateral surface of the left dentary (Fig. 2).

The left maxilla lacks the nasal process, and only a small posterior fragment of the right bone is preserved (Fig. 3). The antorbital fenestra length is only 105.7% of its height (measured in the posterior portion, just in front of the lacrimal), in contrast to the elongated condition seen in *Velociraptor mongoliensis*, *Linheraptor exquisitus*, and *Tsaagan mangas* (Table 1, Figs. 5, 6). The antorbital fenestra is roughly equal in height and length or taller than longer in *Saurornitholestes langstoni* UALVP 55700, *Sinornithosaurus millenii* IVPP V12811 (Xu and Wu 2001; Currie and Evans 2020), and most likely in *Atrociraptor marshalli* (Powers et al. 2022). The ventral margin of the antorbital fenestra tapers anterodorsally, at an angle equal to 24° (measured between the ventral margin of the antorbital fossa and ventral margin of the antorbital fenestra), which is an angle not observed in any specimen of *V. mongoliensis* (up to 15°); however, it is similar to that of *Bambiraptor feinbergi* AMNH FARB 30556 and *Atrociraptor marshalli* (Burnham et al. 2000; Currie and Varricchio 2004). The ventral margin of the antorbital fossa extends below the dorsal extent of maxillary alveoli, as in *V. mongoliensis*, *Shanag ashile*, and *Saurornitholestes langstoni*, but in contrast to "*Velociraptor*" *osmolskae*, *T. mangas* and *L. exquisitus* (Powers et al. 2022).

Ventrally, there is a single row of a neurovascular (=supralabial) foramina. Similarly, as in *V. mongoliensis* (AMNH FARB 6515, MPC-D 100/54), *L. exquisitus*, and *T. mangas*, there is a groove-like, elongate neurovascular foramen extending above the few posterior alveoli. Just above the row there is a distinct longitudinal labial ridge delimiting the antorbital fossa ventrally (Fig. $3A_7$–A_{10}). The ridge is 4 mm high dorsoventrally and protrudes laterally for a 1.5 mm. The ridge reaches the maxillo-jugal suture posteriorly, being

Table 1. Cranial measurements (in mm) of velociraptorines from the Upper Cretaceous of the Gobi Desert. Most of the measurements follow outlines by Powers et al. 2020, with the exception of the antorbital fenestra height that was measured here in the posteriormost portion of the fenestra. Data after Powers et al. 2020 and personal observations. ?, measurement not possible.

Taxon	*Shri devi*	*Velociraptor mongoliensis*			*Velociraptor* sp.	*Tsaagan mangas*	*Linheraptor exquisitus*	"*Velociraptor*" *osmolskae*
Specimen	ZPAL MgD-I/97	AMNH FARB 6515	MPC-D 100/25	MPC-D 100/54	MPC-D 100/982	MPC-D 100/1015	IVPP V16923	IMM99NM-BYM-3/3
		left/right	left/right	left/right	left/right	left/right	left/right	
Locality	Khulsan	Bayan Zag	Tögrögiin Shiree	Tögrögiin Shiree	Bayan Zag	Ukhaa Tolgod	Bayan Mandahu	Bayan Mandahu
Maxilla								
maxilla length	?	91.0/?	111.9/114.8	96.4/107.9	89.9/98.9	105.2/103.3	117.6/107.8	?
antorbital fossa length	21.0	22.0/24.1	30.2/30.7	27.4/34.6	34.7/30.2	20.1/17.4	28.9/26.1	29.4
antorbital fenestra length	29.5	34.7/34.1	43.6/41.5	35.8/39.0	35.1/35.5	45.9/41.9	32.3/33.8	?
antorbital fenestra height (posterior)	27.9	23.5/?	32.7/32.3	23.2/24.5	24.1/?	?/25.2	21.3/23.3	?
anterior margin of antorbital fossa to maxillary fenestra length	7.2	9.9/11.3	13.5/11.9	10.6/15.2	19.3/19.2	0.0/0.0	0.0/0.0	9.8
maxillary fenestra length	9.4 (e)	7.6/5.7	11.4/11.2	14.0/11.3	6.9/6.2	?/11.8	19.3/21.7	13.3
pila interfenestralis length	4.1	3.9/?	7.2/8.0	4.8/9.0	8.4/10.5	?/5.7	9.9/10.6	6.1
ventral margin height (anterior)	7.6	5.2/7.6	10.3/10.4	8.8/9.9	6.0/6.1	14.7/14.3	16.2/16.2	12.5
ventral margin height (posterior)	4.3	2.6/1.7	4.2/4.5	3.7/3.7	4.7/2.4	11.6/12.7	8.5/9.2	9.8
last maxillary tooth to posterior end of maxilla	4.6	27.2/?	21.8/?	17.3/19.8	?/10.1	17.3/?	13.6/14.9	37.8
Ratios								
antorbital fossa/antorbital fenestra length	0.712	0.634/0.707	0.693/0.740	0.765/0.887	0.989/0.851	0.438/0.415	0.895/0.772	?
antorbital fenestra length/height	1.057	1.477/?	1.333/1.285	1.543/1.592	1.456/?	?/1.663	1.516/1.451	?
maxillary fenestra/antorbital fossa length	0.448	0.345/0.237	0.378/0.365	0.511/0.327	0.199/0.205	?/0.678	0.668/0.831	0.452
pila interfenestralis length/ antorbital fossa	0.195	0.177/?	0.238/0.261	0.175/0.260	0.242/0.348	?/0.328	0.343/0.406	0.207

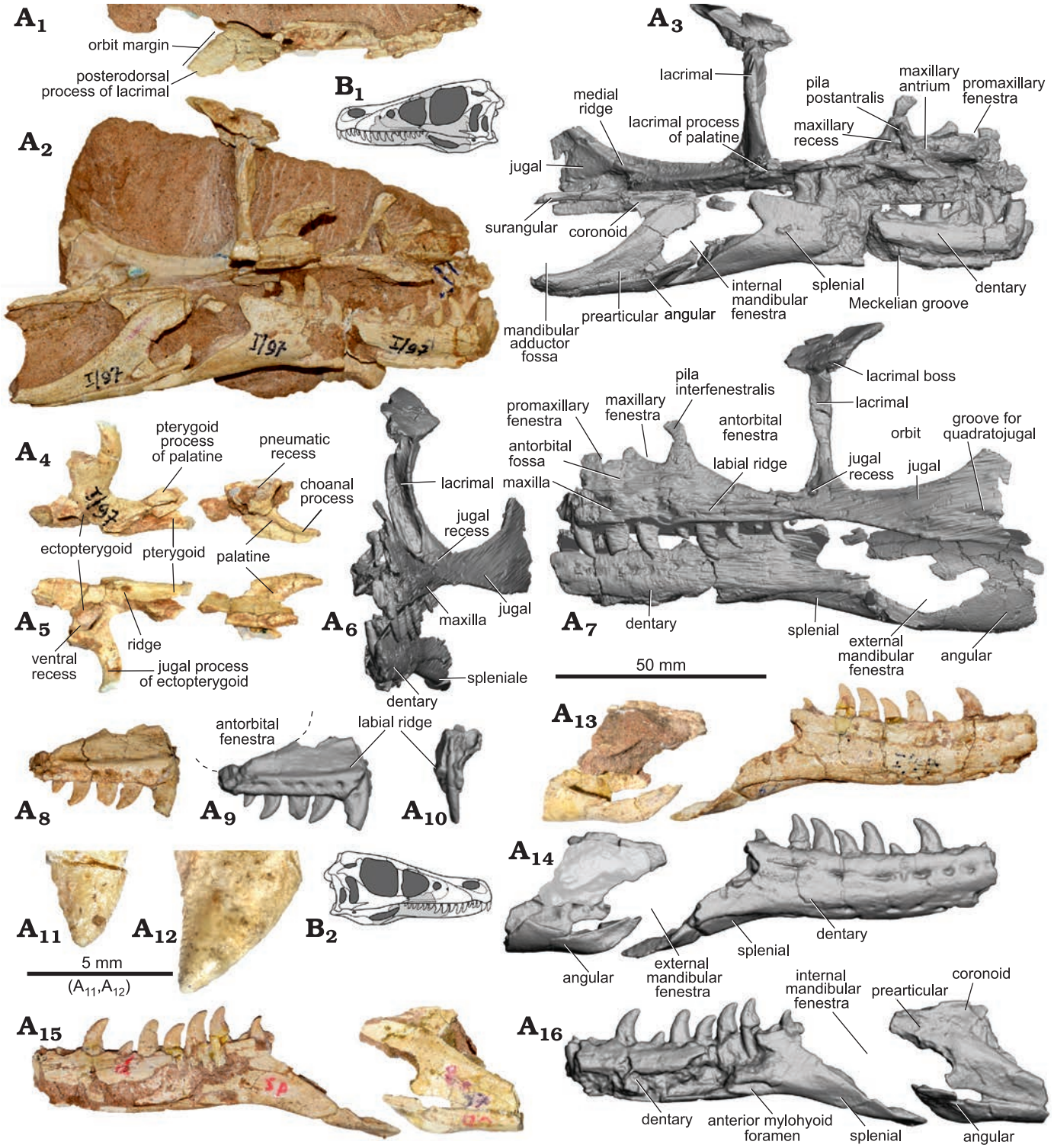

Fig. 3. Dromaeosaurid dinosaur *Shri devi* Turner, Montanari, and Norell, 2021 (ZPAL MgD-I/97) from the Upper Cretaceous, Khulsan, Ömnögovi, Gobi Desert, Mongolia. Photographs (A_1, A_2, A_4, A_5) and 3D model (A_3, A_6, A_7) obtained from the CT scan of the left side of the skull in dorsal (A_1), medial (A_2, A_3), anterior (A_6), and lateral (A_7) views. Elements of the left palate in dorsal (A_4) and ventral (A_5) views. Right maxilla in the lateral (A_8, A_9) and anterior (A_{10}) views, with the margin of the antorbital fenestra indicated by dashed lines, and the close up of the fifth (A_{11}) and the second (A_{12}) preserved tooth in labial views showing very weakly developed denticles on the mesial carina. Right mandible in the lateral (A_{13}, A_{14}) and medial (A_{15}, A_{16}) views. **B**. Explanatory drawings of the skull in left (B_1) and right (B_2) lateral views with the preserved bones (in grey).

much more prominent than the ventral delimitation of the antorbital fossa seen in *V. mongoliensis* (MPC-D 100/25, MPC-D 100/54) and *Velociraptor* sp. (MPC-D 100/982).

Only the anteroventral and posterior margins of the relatively large maxillary fenestra are preserved (Fig. $3A_7$). It is positioned close to the anterior margin of the antorbital

Fig. 4. Dromaeosaurid dinosaur *Shri devi* Turner, Montanari, and Norell, 2021 (ZPAL MgD-I/97) from the Upper Cretaceous, Khulsan, Ömnögovi, Gobi Desert, Mongolia. **A**. Left metatarsus in anterior (A_1, A_2) and posterior (A_3, A_4) views, and phalanges of digit IV (A_5), digit III (A_6), digit II (A_7), and digit I (A_8) in medial views, metatarsal I in anterior view (A_8). Ungual III-4 is presented as a 3D model obtained from the CT scan. **B**. Plot presenting the elongation of II-3 in relation to the length of metatarsal II in dromaeosaurid dinosaurs. Blue dots represent specimens from the Djadokhta strata, orange from the Baruungoyot strata, black from Bayan Mandahu, and white from North America.

fenestra, extending more posteriorly than in some specimens of *V. mongoliensis* (MPC-D 100/25, PIN 3143/8) and *Velociraptor* sp. MPC-D 100/982, resulting in a relatively anteroposteriorly short pila interfenestralis, with a constriction at its dorsoventral midpoint. The greatest longitudinal diameter of the fenestra is 9 mm long, and it equals 44.8% of the distance between the anterior margin of the antorbital fossa and the antorbital fenestra. The precise anteroposterior position and size of the fenestra is known to vary even in a single specimen (it is relatively larger and positioned more caudally on the left side of the MPC-D 100/54; see Table 1). In *L. exquisitus* and *T. mangas* the anterior portion of the maxillary fenestra is tucked into the anterior margin of the antorbital fossa (Norell et al. 2006; Xu et al. 2010). The dorsoventral position of the fenestra is about the midpoint height of the antorbital fenestra in ZPAL MgD-I/97.

Anteriorly, there is a narrow promaxillary fenestra that is constrained into the anterior margin of the antorbital fossa. There are two promaxillary fenestra of a similar size in some specimens of *V. mongoliensis* (MPC-D 100/25, MPC-D 100/54), whereas in AMNH FARB 6515 one fenestra is slit-like and the second one is smaller in size (Barsbold and Osmólska 1999). It is not possible to determine the number and sizes of the promaxillary fenestrae in ZPAL MgD-I/97 as the specimen is incompletely preserved in this area. The promaxillary fenestra is at the level of the ventral margin of the maxillary fenestrae in ZPAL MgD-I/97, similar to *V. mongoliensis* MPC-D 100/25. It differs from the condition seen in *L. exquisitus*, and *T. mangas* where the single promaxillary fenestra is more ventral than the maxillary one (Norell et al. 2006; Xu et al. 2010, 2015). Closely located maxillary and promaxillary fenestrae are also seen in *Achillobator giganticus*, *Atrociraptor marshalli*, and "*V.*" *osmolskae* (Currie and Varricchio 2004; Godefroit et al. 2008; Turner et al. 2012); however, in the latter, the promaxillary fenestra is of similar large size as the maxillary one.

There is no lateral recess posterior to the maxillary fenestra in ZPAL MgD-I/97, in contrast to *Acheroraptor te-*

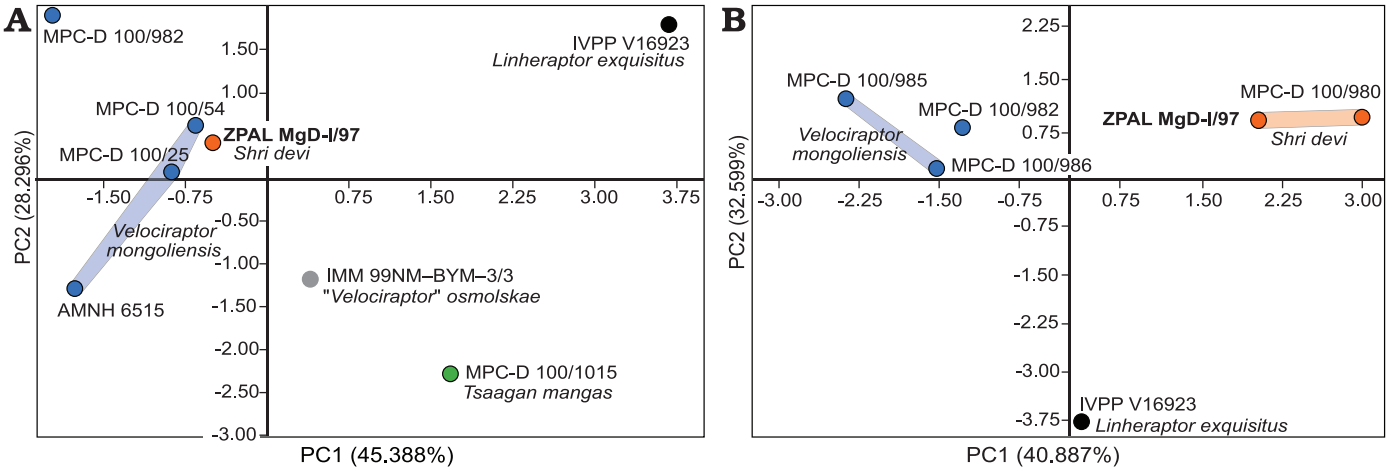

Fig. 5. Results of the PCA for the linear measurements of maxilla (**A**) and pes (**B**) for the velociraptorines from the Upper Cretaceous of the Gobi Desert. Blue dots represent specimens from the Djadokhta strata, orange from the Baruungoyot strata, green from Ukhaa Tolgod, and black and grey from Bayan Mandahu.

mertyorum, *L. exquisitus*, and *T. mangas* (Evans et al. 2013; Xu et al. 2015; Brownstein 2021). Such a structure is related to the development of the postantral wall (additional maxillary pneumatic fenestra sensu Brownstein 2021). However, as the pila postantralis is positioned relatively more anteriorly in ZPAL MgD-I/97 than in "*V.*" *osmolskae*, and given the preserved portion of the postantral wall, that leans medioventrally, it is possible that in *S. devi* the postantral wall was less visible in the lateral view than in other dromaeosaurids.

Ventral to the antorbital fossa, the maxilla is as low as in *V. mongoliensis*, but unlike *L. exquisitus* and *T. mangas*. It tapers posteriorly as in other velociraptorines. The ventral margin of the maxilla is nearly straight below the antorbital fossa, as in most of the *V. mongoliensis* specimens (except MPC-D 100/54).

The Z-shaped suture between the maxilla and jugal is visible in lateral view. The dorsal portion of the suture directs posteroventrally, while at the level of the ventral margin of the antorbital fossa it abruptly projects anteriorly, and below the labial ridge again continues posteroventrally (Fig. $3A_6$–A_7). In *V. mongoliensis* (AMNH FARB 6515, MPC-D 100/25, MPC-D 100/54), *L. exquisitus* (IVVP V1692) and *T. mangas* (MPC-D 100/1015) there is a simple suture with the maxillary process of the jugal overlapping the maxilla dorsally. The longitudinal notch on the posterior part of the jugal ramus of the *Atrociraptor marshalli* TMP 1995.166.0001 maxilla suggests the presence of the Z-shaped suture (Currie and Varricchio 2004; Powers et al. 2022). that is also visible on the left side of the specimen of *Saurornitholestes langstoni* UALVP 55700 (Currie and Evans 2020).

The preserved part of the jugal, which is missing its dorsal and posterior regions, measures 59.5 mm. The bone is triangular in lateral view, and is distinctly deeper in the posterior portion. Contribution of the jugal to the margin of the antorbital fenestra is very limited. Similar to *V. mongoliensis*, there is no dorsoventral constriction at the contact between maxilla and jugal in ZPAL MgD-I/97, observed in *L. exquisitus*. In the posteroventral corner of the antorbital fossa, just below the contact with the lacrimal, there is a distinct fossa, the jugal pneumatic recess (sensu Witmer 1997), similar to that in *V. mongoliensis* (MPC-D 100/54, see also: Barsbold and Osmólska 1999) and *T. mangas* (Norell et al. 2006). CT data reveals that this recess deeply penetrates the suborbital ramus of the jugal to the level of the midpoint of the orbit. It differs from the apparently solid suborbital ramus of the jugal in *Tsaagan* (Norell et al. 2006). The ventral margin of the jugal bone in ZPAL MgD-I/97 projects posteroventrally in the lateral view for the majority of the orbital length. In *V. mongoliensis* (MPC-D 100/25, MPC-D 100/54, PIN 3143/8), and *Velociraptor* sp. MPC-D 100/982 the ventral margin projects nearly parallel to the ventral margin of the orbit for nearly its whole length. In contrast, the ventral margin of the jugal of *L. exquisitus* projects much more posteroventrally. The orbital margin of the jugal is slightly concave in ZPAL MgD-I/97, similar as in *V. mongoliensis* and *T. mangas*. In some specimens of *V. mongoliensis* it is straight, similar as in *L. exquisitus*, while being slightly convex in the midlength of *Adasaurus mongoliensis* MPC-D 100/20.

In ZPAL MgD-I/97, the lateral surface of the jugal is smooth and flat. The ventral margin is thin, in contrast to the condition seen in *Adasaurus mongoliensis* (MPC-D 100/20), *L. exquisitus*, and *V. mongoliensis* (AMNH FARB 6515, MPC-D 100/24, 25, PIN 3143/8), where a longitudinal ridge is present, parallel to the ventral margin of the postorbital process of the jugal. Near the ventral margin of the jugal there is a shallow longitudinal groove in ZPAL MgD-I/97. It is most likely the anteriormost portion of the groove receiving the jugal process of the quadratojugal. If interpreted correctly, this would mean that either the jugal bone was relatively short anteroposteriorly in ZPAL MgD-I/97 or the jugal process of the quadratojugal was relatively long. In any case, the quadratojugal recess is not present anterior to the posterior orbital margin of the jugal in any other velociraptorine specimen (Fig. 7). The only exception may be *Adasaurus mongoliensis* (MPC-D 100/20), where there

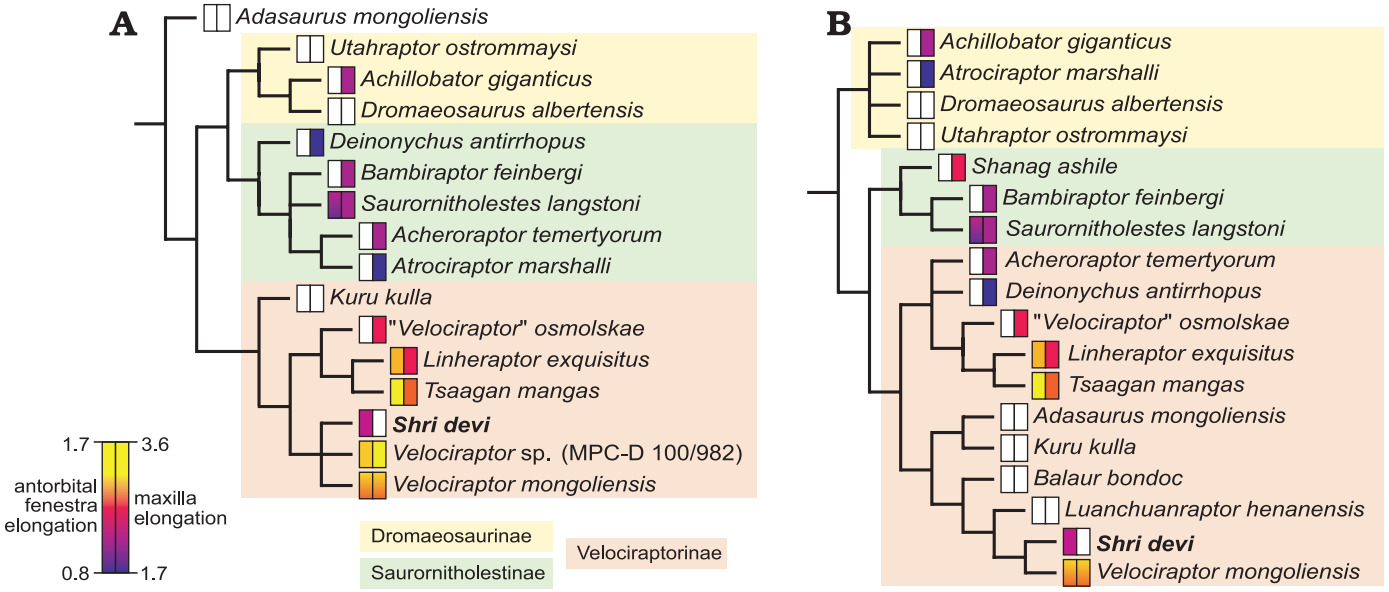

Fig. 6. Phylogenetic relationships of *Shri devi* Turner, Montanari, and Norell, 2021, among the dromaeosaurid dinosaurs. Values of the antorbital fenestra elongation (measured as the ratio of the posterior margin height to the longitudinal length) and elongation of the maxilla (measured as the ratio of the maxilla length to its height; data after Powers et al. 2022) are mapped on the 50% majority rule consensus trees generated from the modified data matrices of Powers et al. 2022 (**A**), and Napoli et al. 2021 (**B**). White rectangles represent the missing data.

is a longitudinal groove developing in the posterior part of the jugal, dorsally to the ventral margin of the bone, nearly reaching the level of the midlength of the orbit. The contact with the quadratojugal is positioned dorsal to the level of the alveolar maxillary margin, similar as in *V. mongoliensis* and *Velociraptor* sp. (MPC-D 100/982), in contrast to *L. exquisitus* and *T. mangas*, where it lies significantly more ventrally. In medial view, there is a robust ridge on the jugal, extending to the level of the contact with the ectopterygoid (Fig. $3A_2$, A_3), which was also reported in other dromaeosaurids (Xu et al. 2015). In the posterior part, in the region of the postorbital process of the jugal, there is an extensive concavity below the medial longitudinal ridge. In the anterior corner there is a contact surface for the ectopterygoid.

The lacrimal is T-shaped in lateral view, similar to that in other dromaeosaurids. The anterior process of the lacrimal bone is not preserved, and the posterior process is very short (Fig. $3A_1$) when compared to *Kuru kulla* (MPC-D 100/981), *L. exquisitus*, *Saurornitholestes langstoni*, *T. mangas*, and *V. mongoliensis.* It results in the contact between the lacrimal and frontal being positioned more anteriorly in ZPAL MgD-I/97 than in other dromaeosaurids. The lateral margin of the posterior process directs acutely posteromedially in ZPAL MgD-I/97, forming an angle of 49° with the longitudinal axis of the skull when seen in the dorsal view. It differs from the condition seen in *V. mongoliensis* where the lateral margin of the lacrimal is directed more posteriorly than posteromedially (in range from 18° in MPC-D 100/24 to 28° in MPC-D 100/25). The dorsal surface is flat and is dorsally inclined posteromedially to the much greater degree than in *Velociraptor* sp. (MPC-D 100/982) and *K. kulla* (MPC-D 100/981). There are several small foramina on the dorsal surface, similar as in *L. exquisitus* (Xu et al. 2015) and *V. mongoliensis* (MPC-D 100/54) (see also Brownstein 2021). Just above the lacrimal shaft there is a shallow longitudinal convexity in ZPAL MgD-I/97. The lateral and orbital edges bear small rugosities, overhanging the ventral process of the bone.

Posterolaterally, there is a small projection, a lacrimal boss (Fig. $3A_1$, A_6, A_7), similar to that seen in *V. mongoliensis* (AMNH FARB 6515, MPC-D 100/25, MPC-D 100/54), *L. exquisitus*, "*Velociraptor*" *osmolskae*, *Bambiraptor feinbergi* (AMNH FARB 30556), *Deinonychus antirrhopus* (YPM 5232), and *Utahraptor ostrommaysorum* (Kirkland et al. 1993; Godefroit et al. 2008; Xu et al. 2015). *Kuru kulla* (MPC-D 100/981, Napoli et al. 2021) has a small but very distinct lacrimal hornlet, that is positioned more dorsally, while *Tsaagan mangas* purportedly lacks the lacrimal boss (Norell et al. 2006; Xu et al. 2015). The bone is highly pneumatized with the pneumatic foramen of the lacrimal recess (sensu Witmer 1997) present in the posterodorsal corner of the antorbital fossa, dorsal to the distinct lacrimal duct.

In lateral view the ventral process of lacrimal is nearly vertically oriented, different from what is seen in *Adasaurus mongoliensis* (MPC-D 100/20) where the bone is arched anteroventrally. The bone is relatively straight in *V. mongoliensis* (AMNH FARB 6515, MPC-D 100/25, PIN 3143/8) and *Linheraptor* while being slightly curved in *V. mongoliensis* (MPC-D 100/54) and *Velociraptor* sp. (MPC-D 100/982). In anterior and posterior view the bone is more laterally concave than in other velociraptorines (Fig. $3A_6$). The contact with the maxilla is restricted by the maxillary process of the jugal (Fig. $3A_3$). The ventral process is thin ventrally in the lateral view, but extends anteroposteriorly in the dorsal half of the lacrimal in ZPAL MgD-I/97. It differs from the condition of the anteroposteriorly thin lacrimal ventral pro-

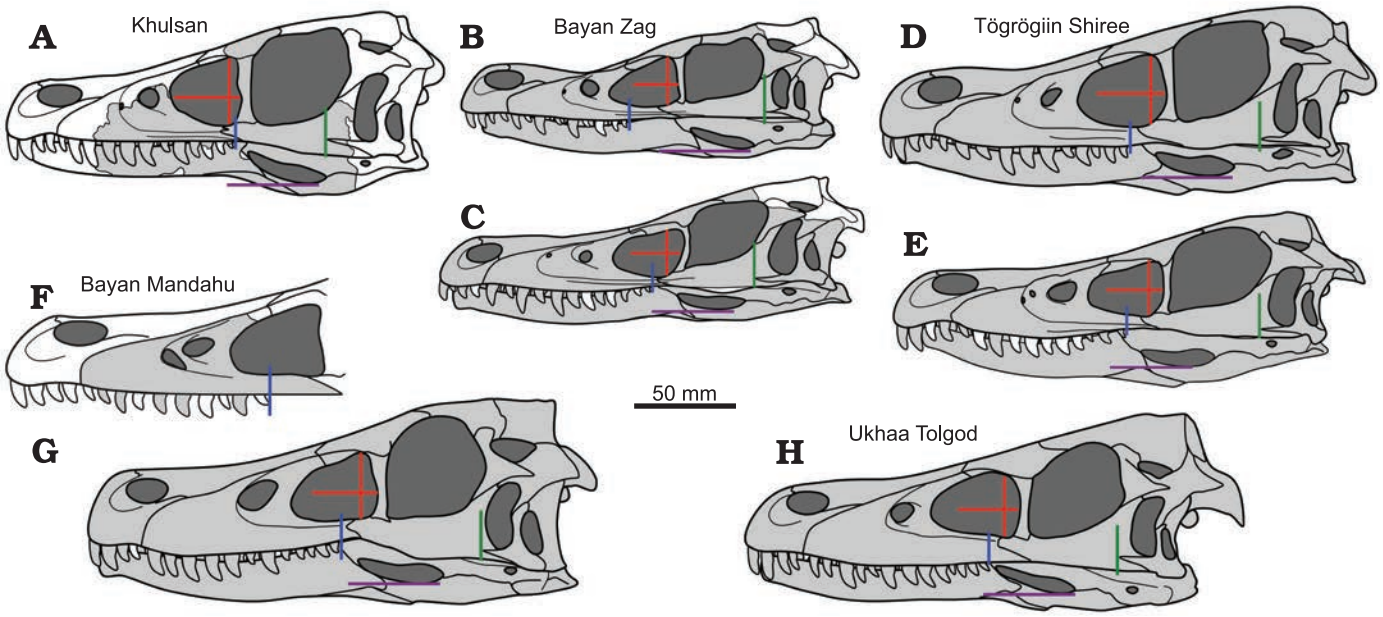

Fig. 7. Comparison of silhouettes of the velociraptorine skulls from different sites of the Upper Cretaceous of the Gobi Desert. **A**. *Shri devi* Turner, Montanari, and Norell, 2021, ZPAL MgD-I/97. **B**, **D**, **E**. *Velociraptor mongoliensis* Osborn, 1924. **B**. AMNH FARB 6515. **D**. MPC-D 100/25. **E**. MPC-D 100/54. **C**. *Velociraptor* sp. MPC-D 100/982. **F**. "*Velociraptor*" *osmolskae* Godefroit, Currie, Li, Shang, and Dong, 2008, IMM 99NM-BYM-3/3. **G**. *Linheraptor exquisitus* Xu, Choinere, Pittman, Tan, Xiao, Li, Tan, Clark, Norell, Hone, and Sullivan, 2010, IVPP V16923. **H**. *Tsaagan mangas* Norell, Clark, Turner, Makovicky, Barsbold, and Rowe, 2006, MPC-D 100/1015. Known elements from any side of the specimen are in grey. Lines present some of the features distinguishing *S. devi* from other velociraptorines: the maximum height of the antorbital fenestra and its perpendicular projection showing elongation of the fenestra (red lines), the position of the last maxillary alveoli (blue), the anteriormost projection of the quadratojugal (green), and the position of the ventral margin of the external mandibular fenestra (purple).

cess visible in *V. mongoliensis* and *Velociraptor* sp. (MPC-D 100/982); however, does not expand anteroposteriorly to the degree visible in *L. exquisitus* or "*V.*" *osmolskae*. The lateral lamina is somewhat sinuous in lateral view, with the anterior margin protruding slightly anteriorly than the medial lamina in ZPAL MgD-I/97. In *Velociraptor* and *Linheraptor*, the lateral lamina is more or less parallel to the medial one.

The palate of ZPAL MgD-I/97 was described in detail by Barsbold and Osmólska (1999). It preserves elements of palatine, pterygoid, vomer, and ectopterygoid (Fig. 3A$_4$, A$_5$).

The pterygoid bears a distinct longitudinal ridge on its ventral surface (Fig. 3A$_5$), as was reported for *Linheraptor* (Xu et al. 2015). Medial to it there is a shallow fossa, that however is not flush with the ventral ectopterygoid recess. A partial left palatine is preserved in ZPAL MgD-I/97 (Fig. 3A$_4$, A$_5$) including the choanal process with a distinct longitudinal fossa on its dorsal surface. On the dorsal surface, along the contact with maxilla there is a pneumatic recess. Anterolaterally there is a short maxillary process. The elongated lacrimal process of the palatine contacts with the lacrimal, overlaps the posterior ramus of maxilla. The elongated pterygoid process of the palatine overlaps dorsally the anterior part of the nearly completely preserved ectopterygoid (Fig. 3A$_4$, A$_5$). Ventrally there is a ventral recess (sensu Witmer 1997) on ectopterygoid consisting of two fossae with a low crest separating them on the posterior wall of the recess (see Barsbold and Osmólska 1999). There is no dorsal ectopterygoid recess in ZPAL MgD-I/97 unlike that reported to be present in *V. mongoliensis* (MPC-D 100/25, MPC-D 100/54), *L. exquisitus*, and possibly *Velociraptor* sp. (MPC-D 100/982), while absent in *T. mangas* (Norell et al. 2006; Xu et al. 2015). The bone seems to be less robust than that in *V. mongoliensis* (MPC-D 100/25, MPC-D 100/54).

The dentary (Fig. 3A$_3$, A$_7$, A$_{13}$–A$_{16}$) is dorsoventrally low in ZPAL MgD-I/97 (with its height equal to 16 mm), which is similar to *V. mongoliensis.* The anteriormost portion of the dentaries are not preserved in the specimen. The dorsal and ventral margins are nearly parallel to each other. The bone is gently bowed ventrally in lateral view, as in *V. mongoliensis* and *T. mangas*; however, this is to a lesser degree than observed in *L. exquisitus.* It contrasts with the nearly straight dentary of *K. kulla*. On the lateral surface, the relatively shallow, longitudinal groove housing neurovascular foramina along the dorsal margin is present. The second row of the foramina is visible along the ventral margin, and it terminates far more anteriorly than the dorsal one (Fig. 3A$_{14}$). In *K. kulla* (MPC-D 100/981) there is only a dorsal row of the foramina present. The long posteroventral process extends along the lateral surface of the splenial bone. Lingually there is a shallow and wide longitudinal Meckelian groove visible on both dentaries. There is a thin furrow present close to the alveolar margin in the anterior portion of the dentary, that bears a row of foramina in the anteriormost portion, as noted by Barsbold and Osmólska (1999). The well-developed, longitudinal anterior mylohyoid

foramen is anterior to the level of the last two dentary teeth which is more anterior than in *T. mangas*.

The splenial is extensively exposed in the lateral view, as in *V. mongoliensis* and other dromaeosaurids. The posterior ramus of the bone with a surface for contact with the angular is directed relatively more posteroventrally than in other velociraptorines. The angular bone contacts the splenial anteriorly, defining the ventral margin of the external mandibular fenestra, and becomes much thinner posteriorly. There is a shallow groove on the lateral surface of the bone, with a very thin crest along the anteroventral margin, next to the contact with the splenial bone. Such a crest is not visible in *T. mangas* nor *L. exquisitus*, but is present in *V. mongoliensis*. The prearticular forms most of the medial region of the mandible posterior to the dentary. Posteriorly, it forms the well-defined anteroventral and ventral margins of the adductor fossa. The small, triangular coronoid is preserved medially on both sides of the specimen, being wedged between the surangular and prearticular.

The ventral margin of the external mandibular fenestra in ZPAL MgD-I/97 seems to extend significantly below the ventral margin of the dentary, as it can be indicated from the morphology of the lateral surface of the angular bone, lower than in *Dromaeosaurus albertensis* (AMNH FARB 5356), *L. exquisitus*, *Saurornitholestes langstoni*, *T. mangas*, *V. mongoliensis*, and *Velociraptor* sp. (MPC-D 100/982). Therefore, the mandible of ZPAL MgD-I/97 was likely deeper posterior to the dentary than in other velociraptorines; however, the contacts between the splenial and angular, as well as between the dentary and surangular, were most likely movable in the velociraptorines, allowing some passive rotation of the anterior portion of the dentary (Barsbold and Osmólska 1999; Norell et al. 2006) and reconstruction of the exact in vivo placement of the bones might be taphonomically vulnerable.

The surangular bone is only partially preserved on the left side of the specimen (Fig. $3A_3$, A_7). It is very thin in lateral view, being eroded at the level of the dorsal margin of the external mandibular fenestra. No posterior parts of the bone are preserved; hence it is not possible to compare it with the surangular of the *K. kulla* MPC-D 100/981 also known from Khulsan (Napoli et al. 2021), although the surangular shelf seems to be less developed in ZPAL MgD-I/97.

The posteriormost nine maxillary teeth are preserved with the left maxilla and the posterior six (without the posteriormost one) with the right one. The largest maxillary teeth of ZPAL MgD-I/97 are 8.8–10.4 mm in apical length (measured from the most mesial point of the tooth crown base to the crown apex). Gaps between the tooth crown bases are 1.4–3.5 mm posteroventrally. Tooth roots are mediolaterally compressed, as in other velociraptorines. Approximately each second tooth is bigger than the preceding one, making a series of teeth differing in size, as seen in *V. mongoliensis* (Barsbold and Osmólska 1999). It seems that such tooth replacement pattern is less strict in ZPAL MgD-I/97, as the second and third preserved teeth of the left maxilla are of relatively similar, large size (as estimated by the widths at the bases of the teeth). As a result, the second, third, fifth, and seventh preserved teeth are the largest. However, it also varies within the *V. mongoliensis* sample and the clear pattern representing the alternating cycles of tooth replacement (Barsbold and Osmólska 1999; Norell et al. 2006) is seen only in few specimens. In "*Velociraptor*" *osmolskae*, the maxillary teeth differ in size to some degree (Godefroit et al. 2008), while in *L. exquisitus* and *T. mangas* the maxillary teeth are of similar size, with the anterior teeth being generally larger than the posterior ones. However, in *Tsaagan* the alternating pattern is visible within dentary teeth (Norell et al. 2006; Xu et al. 2015).

In ZPAL MgD-I/97 the last maxillary tooth is positioned posterior to the anteriormost extent of the maxillo-jugal suture, just in front of the level of the lacrimal (Fig. $3A_2$, A_3, A_7). It differs from the condition seen in other eudromaeosaurians, where most of the maxilla posterior to the midpoint of the antorbital fenestra is edentulous, with exception for *Atrociraptor marshalli* and *Saurornitholestes langstoni* (UALVP 55700). In *V. mongoliensis* the maxillary teeth usually are not present below the posterior half of the antorbital fenestra (e.g., AMNH FARB 6515, MPC-D 100/25; Table 2). On the left side of the *T. mangas* (MPC-D 100/1015), and in *Velociraptor* sp. (MPC-D 100/982), the last maxillary tooth is preserved relatively posteriorly, but not to the degree seen in ZPAL MgD-I/97. In "*V.*" *osmol-*

Table 2. Teeth of velociraptorines from the Upper Cretaceous of the Gobi Desert.

Taxon	Specimen	Total tooth number	Teeth posterior to antorbital fossa	Teeth posterior to antorbital fenestra
Shri devi	ZPAL MgD-I/97	?	8	5
Velociraptor mongoliensis	AMNH FARB 6515	10	5	2
	MPC-D 100/24	11	8	4
	MPC-D 100/25	11	8	4
	MPC-D 100/54	11	7	3
	MPC-D 100/1252	10	7	?
Velociraptor sp.	MPC-D 100/982	12	8	4
Tsaagan mangas	MPC-D 100/1015	13	8	4
Linheraptor exquisitus	IVPP V16923	12	6	3
"*Velociraptor*" *osmolskae*	IMM99NM-BYM-3/3	?10	?7	?4

skae ten maxillary teeth were reported (Godefroit et al. 2008) and the last one seems to be present somewhere proximal to the midlength of the antorbital fenestra. In *Linheraptor exquisitus*, the last tooth is below the proximal third of the antorbital fenestra.

There are ten teeth preserved in the right dentary and nine in the left one. The longest dentary teeth are 8 mm long and spaces between the alveoli are 2–3 mm wide. The last dentary tooth is anterior to the last maxillary tooth.

Both labial and lingual surfaces of maxillary and dentary teeth are smooth, without the longitudinal ridges (sensu Hendrickx et al. 2015) visible on labial surfaces of some of the maxillary teeth of *V. mongoliensis* (AMNH FARB 6515, MPC-D 100/54). There are about 4.5–5, and 5–5.5 denticles per millimeter on the distal carinae of maxillary and dentary teeth of ZPAL MgD-I/97, respectively. The denticles are simple and perpendicularly oriented in relation to the longer axis of the tooth. The mesial surface of the teeth is often rounded, similar to *L. exquisitus* and *T. mangas*. Only on the second and fifth preserved tooth of the right maxilla there is a very weakly preserved mesial serration (Fig. $3A_{11}$, A_{12}). The presence of the mesial serration only on some teeth is visible also in another velociraptorine specimen from the Baruungoyot strata, ZPAL MgD-I/102, while being absent in some isolated teeth collected from Khulsan (ZPAL MgD-I/200). It suggests that the feature of presence of the mesial denticles may be more related to the taphonomic conditions than reflecting the diagnostic differences between the taxa (see also Barsbold and Osmólska 1999).

Only an incomplete distal portion of the thin left fibula is preserved in ZPAL MgD-I/97. It is attached to the lateral side of the tibia. It is 5.5 mm wide and subtriangular in cross-section. Its distalmost portion is not preserved. Only a distal portion of the left tibia is preserved (SOM: fig. 1). It is 31 mm wide just above the calcaneum, and its shaft is 23.5 mm wide above the ascending process of the astragalus. The tibia is flattened anteroposteriorly, with a depth equal to 15.5 mm.

The astragalus bears an ascending process (SOM: fig. 1). The process is taller laterally (33.9 mm) than medially (22 mm) and its dorsal extremity slopes medially, giving the bone an overall comma-like shape, similar to that in the holotype of *Shri devi* (MPC-D 100/980; Turner et al. 2021), *V. mongoliensis* (MPC-D 100/986; Norell and Makovicky 1999), and *L. exquisitus* (IVPP V16923). Distally, the ascending process of the astragalus covers all of the anterior wall of the distal end of tibia. The body of the astragalus is not completely preserved. On the anterior wall of the ascending process of the astragalus, above the basal body, there is a distinct lateromedial groove. The preserved portion of the lateral condyle suggests that the astragalus and calcaneum were not fused to each other, similar to *Achillobator giganticus*, *L. exquisitus*, and *Deinonychus antirrhopus*, but in contrast to *Adasaurus* and *V. mongoliensis*. Only a small portion of a calcaneum is preserved on ZPAL MgD-I/97. Although the elements of the hindlimb are articulated, the distal tarsals and calcaneum are not preserved.

The first four metatarsals of the left pes are almost completely preserved in articulation (Figs. 2, $4A_1$–A_4), lacking only their proximalmost extremities. The preserved length along the third metatarsal is 91 mm, whereas the proximal width of the combined metatarsals II–IV is 32.7 mm. The metatarsal I is the shortest one (Fig. $4A_8$). It tapers proximally, among its arched shaft. The flat portion of the lateral surface indicates its contact with the shaft of the second metatarsal. Distally there is a nonarticular shaft of the bone present, similar as in *S. devi* (MPC-D 100/980), but not present in *K. kulla* (MPC-D 100/981). The shallow ligament pit is present only on the lateral surface, with no trace of the medial ligament pit, condition similar to *S. devi* (MPC-D 100/980) and *V. mongoliensis* (Norell and Makovicky 1997), in contrast to *K. kulla* (MPC-D 100/981, Napoli et al. 2021). The articular surface is divided by a gentle fossa. The bone has a very shallow longitudinal fossa on the lateral surface, distal to the articulation with metatarsal II, even less distinct than the one in *S. devi* (MPC-D 100/980, Turner et al. 2021), and much shallower than in *V. mongoliensis* (AMNH FARB 6518, MPC-D 100/985, MPC-D 100/986; Norell and Makovicky 1997).

The metatarsal II is shorter than the third and fourth ones. In the anterior view, the shaft of the second metatarsal is nearly rectangular, with a longer anteroposterior axis than a mediolateral one. Its contact with the metatarsal I is positioned distal to the midline of the bone's shaft, as in most coelurosaurs, including the majority of *V. mongoliensis* specimens (Norell and Makovicky 1997, 1999). An exception is MPC-D 100/986 *V. mongoliensis* from Chimney Buttes, where the attachment site for metatarsal I is more proximal (Norell and Makovicky 1999; Hattori 2016). Proximally, metatarsal II is wider than metatarsal III. Although the proximalmost portion of the metatarsal II is not preserved in ZPAL MgD-I/97, this condition is similar, although less prominent, to *S. devi* (MPC-D 100/980), *L. exquisitus* (IVPP V16923), and *Deinonychus antirrhopus*, and differs from a very thin proximally metatarsal II of *Adasaurus mongoliensis* (MPC-D 100/21), *K. kulla* (MPC-D 100/981), and *V. mongoliensis* (MPC-D 100/54, 100/985, 100/986, with exception of MPC-D 100/25, where the preserved part of the right pes suggests a proximally constricted metatarsal III). On the anterior surface there is a small tubercle present near the contact with metatarsal III (Fig. $4A_1$, A_2), suggested as the attachment site for M. tibialis cranialis by Norell and Makovicky (1997). In ZPAL MgD-I/97 it is positioned laterally, as in *S. devi* (MPC-D 100/980), and *L. exquisitus* (IVPP V16923), whereas in *V. mongoliensis* it is located more centrally. On the posterior surface, near the medial margin there is a subtle longitudinal tubercle, near the contact with metatarsal I, a medial plantar crest sensu Norell and Makovicky (1997) (Fig. $4A_3$, A_4). In ZPAL MgD-I/97 it is less prominent than the one observed in *S. devi* (MPC-D 100/980). Just above the ging-

lymoid distal articulation, the shaft of the metatarsal II is slightly narrower in ZPAL MgD-I/97, similar to *V. mongoliensis* (MPC-D 100/985, MPC-D 100/986) but unlike the condition of a constant width of the bone's shaft in *S. devi* (MPC-D 100/980, Turner et al. 2021). The lateral hemicondyle is slightly larger than the medial one, which twists medially more distinctly than in *S. devi* (MPC-D 100/980), *V. mongoliensis* (MPC-D 100/985) (see Norell and Makovicky 1997) or *L. exquisitus*.

Metatarsal III is the longest one, being slightly compressed lateromedially by adjacent bones. The preserved proximalmost portion is subrectangular in cross-section and the lateroventral region is elongated anteroposteriorly. The proximalmost width of the third metatarsal is narrower than the adjacent metatarsals. On the anterior surface, there is a small, weakly developed longitudinal tubercle on the lateral margin of the bone (Fig. $4A_1$, A_2), proximal to the distal articulation, as in the *S. devi* holotype (MPC-D 100/980) and in *L. exquisitus* (IVPP V16923). A better developed, centrally positioned tubercle is visible in *V. mongoliensis* (MPC-D 100/54, 100/985, 100/986) and *Deinonychus antirrhopus* (YPM 5205, Turner et al. 2021). In ZPAL MgD-I/97 the bone lacks the distinct dorsal ridge covering metatarsal IV at the midlength level of metatarsal II seen in *V. mongoliensis* (MPC-D 100/986) from the Chimney Buttes locality. The distal preginglymoid width of a metatarsal III is 20% wider than the adjacent metatarsals in ZPAL MgD-I/97, similar to *V. mongoliensis* (Norell and Makovicky 1999), while in *L. exquisitus* metatarsal III is nearly two times wider than metatarsal II in that region.

The metatarsal IV is intermediate in length between the metatarsal II and III, as in all velociraptorines. In proximal view it is triangular in cross section, extending laterally with a ventrolateral flange, as in *V. mongoliensis* (MPC-D 100/985, 100/986, Norell and Makovicky 1997) and *L. exquisitus*, but not in *S. devi* (MPC-D 100/980, Turner et al. 2021). Proximally, the bone is the widest of all metatarsals. There is a small lateral crest present, the same as the lateral plantar crest reported for *V. mongoliensis* by Norell and Makovicky (1997), where it is positioned just below the proximal articulation, suggesting that the metatarsus is only slightly eroded proximally in ZPAL MgD-I/97. In the distal portion the bone is slightly narrower mediolaterally and projects slightly laterally from the shaft of metatarsal III. The lateral margin of the bone is concave, similar to *V. mongoliensis* (Norell and Makovicky 1997).

All pedal phalanges are preserved and are fairly complete in ZPAL MgD-I/97 (Fig. $4A_5$–A_8). The distal margin of the phalanx I-1 exceeds the distal margin of the second metatarsal when in articulation with the first metatarsal, similar to *V. mongoliensis* MPC-D 100/985 (Norell and Makovicky 1997). There is a small plantar crest extending posteriorly and overlapping the articular surface of the first metatarsal, similar to *V. mongoliensis* (Norell and Makovicky 1997). The plantar surface of the crest is flat in ZPAL MgD-I/97, whereas it has a small tubercle in *V. mongoliensis* MPC-D 100/985. Both the medial and lateral ligament pits are distinct on the distal head. The ungual of the first digit is nearly equal to the I-1. It is oval in the proximal, and weakly curved in the lateral view. On both sides there are distinct grooves for the claw sheath along nearly the whole length of the bone.

Phalanx II-1 (Fig. $4A_7$) is shorter than II-2, as in *S. devi* (MPC-D 100/980) and *V. mongoliensis*, but in contrast to the elongated II-1 in *Adasaurus mongoliensis* (MPC-D 100/21) and *Kuru kulla* (MPC-D 100/981). The proximal portion of the bone is dorsoventrally compressed in lateral view. On the proximal surface, there is a proximoventral keel. It was reported for *V. mongoliensis* (MPC-D 100/985) that such a tongue is connected with a distal medial trochlea by a ridge (Norell and Makovicky 1997). In ZPAL MgD-I/97 there is only a short ridge present on the medial side of the ventral keel, similar to that in MPC-D 100/980 (Turner et al. 2021). Relatively deep ligament fossae are present on both sides of the distal articulation, just above the midpoint of the trochlear dorsoventral height. A shallow but distinct hyperextensor fossa is present on the dorsal surface, in contrast to the weakly developed extensor tendon pit reported for *K. kulla* (MPC-D 100/981, Napoli et al. 2021). The lateral hemicondyle is slightly wider than the medial one. Phalanx II-2 has an asymmetrical proximoventral keel, as in other dromaeosaurids. On the proximal surface of the bone there is an extensive ventral keel, and the distal trochlea are very narrow, with an extensive ginglymoid, as in other dromaeosaurids (Norell and Makovicky 2004). The medial ridge is present on the ventral surface of the keel. Ligament fossae on the distal articular surface are very small and positioned dorsally. The lateral hemicondyle has larger size and is positioned more distally than the medial one. There is no extensor tendon pit visible.

The ungual of the second digit is relatively hypertrophied. Its outer curvature is equal to 80 mm, being 104.2% of the second metatarsal length, more similar to the holotype of *S. devi* (MPC-D 100/980) than *V. mongoliensis* (Fig. 4B; see SOM). The ungual cross section is very narrow. The flexor tubercle, positioned near the ventral border of the articular surface is relatively large and robust. Grooves for the claw sheath are present on both sides of the ungual, with the lateral one positioned more dorsally than the medial one, as in other dromaeosaurids (Kirkland et al. 1993; Norell and Makovicky 1997). In the distal region the lateral groove is located dorsally and is even visible on the medial side, near the claw tip, whereas the medial groove ends anterior to the distal 1/8 of the bone. In *L. exquisitus* the second digit ungual is not completely preserved, but seemingly it was more robust proximally than in *V. mongoliensis*, and less hypertrophied than in MPC-D 100/980 and ZPAL MgD-I/97. It was reported that the second digit ungual was relatively reduced in *K. kulla* (MPC-D 100/981), suggesting its close affinities with *Adasaurus mongoliensis* (Napoli et al. 2021). Despite that the femora of *K. kulla* (MPC-D 100/981) and *S. devi* (MPC-D 100/980) are of similar size, all the phalanges of the former are significantly smaller. However, given the relative sizes of the ungual II-3 and phalanx II-2 in *K. kulla* (MPC-D 100/981)

being similar to that seen in *V. mongoliensis* and *S. devi*, *K. kulla* clearly differs from the condition seen *Adasaurus mongoliensis*, where only the ungual II-3 is reduced.

Phalanx III-1 (Fig. $4A_6$) is the second longest phalanx of the pes. In the proximal view the bone is nearly rectangular in cross section, and is only slightly skewed medially, similar to *V. mongoliensis* (MPC-D 100/985, Norell and Makovicky 1997). Just above the distal trochlea, the relatively large extensor fossa is present. The distal articular surface is ginglymoid and the medial hemicondyle is greater in size than the lateral one. The collateral ligament pits are distinct and positioned at the midpoint of the trochlea. The dorsomedial inclination of the trochlear ridges, reported in *V. mongoliensis* (Norell and Makovicky 1997) are not observed here, as the lateral trochlea is inclined dorsolaterally. Phalanx III-2 is much shorter than III-1 and is similar in length as II-2. The proximal portion in the plantar view is more developed medially, responding to the distal asymmetry of III-1. In the proximal view, both III-2 and III-3 lean laterally, in contrast to the medially skewed condition in *V. mongoliensis* (MPC-D 100/985, Norell and Makovicky 1997). The distal articular surface of III-2 is ginglymoid, with a slightly wider lateral trochlea than the medial one; however, the latter is oriented more distinctly outwarded medially. The medial collateral ligamentar fossa is shallower than the lateral one, and both are positioned slightly above the center of the trochlea. Phalanx III-3 is similar in length to III-2 but is narrower. A very small tubercle is present proximally on the lateral side of the plantar surface. An extensor fossa is not visible on the dorsal surface. The collateral ligament fossae are small, especially the medial one, which is slit-like and positioned near the dorsal margin of the bone. The lateral ligament fossa is oval, deeper, and positioned only slightly below the level of the medial one. Ungual III-4 is preserved in the slab with the left side of the skull (Fig. $3A_2$). It was digitally removed from the rock matrix (Fig. 7C). It is weakly curved and has a small flexor tubercle. Its relative size is similar to that seen in other velociraptorines.

Phalanx IV-1 (Fig. $4A_5$) is slightly shorter than III-1. It is gently arched medially, especially in its distal portion. There is no distinct lateral crest on the proximal articular surface, seen in *V. mongoliensis* (MPC-D 100/985). In the proximal view, the bone is skewed medially, for accommodation of the asymmetrical metatarsal IV, similar as in *V. mongoliensis* MPC-D 100/985. In plantar view there is a longitudinal ridge present at the proximal lateral margin, but no medial ridge visible in *V. mongoliensis* (MPC-D 100/986). The distal articulation is ginglymoid, and the extensor fossa is relatively large. The lateral ligament fossa is deeper than the medial one. Phalanx IV-2 is skewed laterally in the proximal view. The flexor fossa is shallow. Phalanges IV-3 and IV-4 are symmetrical in the proximal view. No differences in slope of the lateral and medial articular surface are seen, in contrast to *V. mongoliensis* MPC-D 100/985. The phalanges are nearly of the same length, with IV-4 being much narrower. The ungual of the fourth digit is not completely preserved, being weakly curved, with a small, but distinct flexor tubercle. The grooves for the claw sheath are positioned at the same level on both sides, and the ventral portion of the ungual is significantly more massive.

Stratigraphic and geographic range.—Type locality and horizon only.

Principal component analysis

Principal component analysis (PCA) was performed for the linear measurements of the maxilla, which seems to be very informative for dromaeosaurids (Currie and Varricchio 2004; Godefroit et al. 2008; Evans et al. 2013; Powers et al. 2020). Here I used the dataset of the maxillary measurements modified from Powers et al. (2020), and the published measurements of the dromaeosaurid pedal bones (Norell and Makovicky 1999; Xu et al. 2010; Turner et al. 2021).

Given data suggest that the antorbital fenestra length seems to be better correlated with the maxillary length in *Velociraptor mongoliensis* ($R^2 = 0.9810$, $p < 0.01$) than the posterior height of the antorbital fenestra ($R^2 = 0.7944$, $p = 0.109$). However, when *Tsaagan mangas* and *Linheraptor exquisitus* are added to the sample, the correlation between these measurements drastically decreases ($R^2 = 0.1273$, $p = 0.4876$; and $R^2 = 0.2159$, $p = 0.353$, for the antorbital fenestra length and height respectively). Hence, while the antorbital fenestra length and height are good predictors of the overall maxillary length in the *V. mongoliensis* sample, the values vary within other velociraptorines. Due to the close resemblance in the anatomy of ZPAL MgD-I/97 and *V. mongoliensis*, the maxillary length was estimated to be about 79 mm for the former specimen. Given that the preserved portion of the left maxilla is 57.2 mm long, it would mean that about ¾ of the maxilla is preserved in ZPAL MgD-I/97. It would suggest that the maxilla of ZPAL MgD-I/97, if its length anterior to antorbital fossa was proportional to that of *V. mongoliensis*, was rather short anteriorly.

Most of the variation in the maxillary measurements (Fig. 5A) are explained by PC1 (45.388%) and PC2 (28.296%). The most important loadings for PC1 are the length of the maxillary fenestra, height of the ventral maxillary ramus and length from the anterior antorbital fossa to the maxillary fenestra, the last one being a negative loading. Specimens of *V. mongoliensis* group together with ZPAL MgD-I/97 along the axis of the PC1. *L. exquisitus* and *T. mangas* were recovered on the positive part of the PC1 axis, mostly due to the proximal migration of the maxillary fenestra within the antorbital fossa, as well as a deep maxilla below the antorbital fossa. Surprisingly, there is high variation in sample of *Velociraptor* spp. with most of the specimens grouping together with ZPAL MgD-I/97 along the PC2 axis, with a distinct placement of the AMNH FARB 6515 and MPC-D 100/982, both collected from the Bayan Zag site. The most

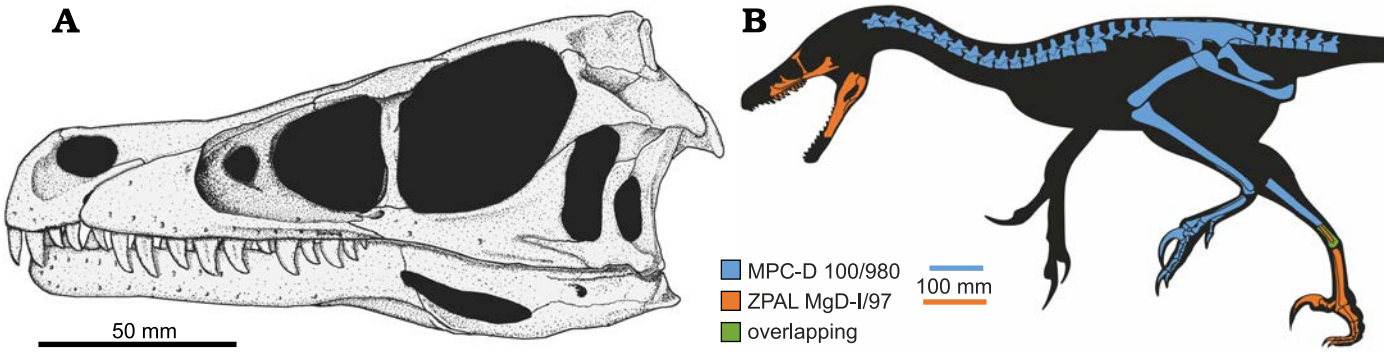

Fig. 8. Reconstruction of the dromaeosaurid dinosaur *Shri devi* Turner, Montanari, and Norell, 2021, based on ZPAL MgD-I/97 and MPC-D 100/980. **A**. Skull; missing elements reconstructed on the base of *Velociraptor mongoliensis* Osborn, 1924 (MPC-D 100/25 and MPC-D 100/54). **B**. Whole body silhouette with known remains of the holotype and referred material. Silhouette based on *V. mongoliensis* drawn by J.A. Headden (Wikimedia Commons CC-BY-3.0).

important loadings for the PC2 are length of the antorbital fossa, anteroposterior width of the pila interfenestralis and position of the most posterior maxillary tooth. MPC-D 100/982 has a significantly elongate antorbital fossa and subsequently the pila interfenestralis is relatively wide due to the central placement of the maxillary fenestra, and it was suggested that the specimen may represent a distinct species (Powers et al. 2022). *L. exquisitus* and *T. mangas*, sometimes considered synonymous, have even wider distribution than the sample of *V. mongoliensis*.

In the PCA of the pedal measurements (Fig. 5B), PC1 explained 40.887% and PC2 32.599% of the variance. The main positive loadings for PC1 were lengths of the metatarsals, and phalanges III-4, IV-1, IV-3 and IV-4, while length of phalanges II-1 was a main negative load. Lengths of the phalanges II-2, III-2, III-3, IV-2, and IV-3 were positive loads for PC2 while metatarsal II and III were negative ones.

ZPAL MgD-I/97 groups with the holotype of *S. devi* MPC-D 100/980 on the positive axes of both PC1 and PC2. Specimens of *V. mongoliensis* from Djadokhta groups together at the negative axis of the PC1, and the single specimen of *L. exquisitus* is found separately at the negative axis of the PC2, close to the center of axis PC1. Separation within the specimens of *S. devi* and *V. mongoliensis* is mostly due to the relatively elongated phalanges of the digit IV in *S. devi* (see SOM).

Discussion

The material of ZPAL MgD-I/97 and the holotype specimen of *Shri devi* (MPC-D 100/980) overlaps solely in the elements of the opposite pes (Fig. 8B), and the measurements reveal that ZPAL MgD-I/97 was about 80% the size of the holotype. As suggested by both the qualitative and quantitative data, the pes of ZPAL MgD-I/97 resembles MPC-D 100/980 more than any other velociraptorine specimen, and the PCA on the pes elements group them together, separately from *Velociraptor mongoliensis* and *Linheraptor exquisitus* (Figs. 4B, 5B). Both specimens have a particularly elongate ungual on the pedal digit II with the length along the outer curvature being greater than the length of the metatarsal II (Fig. 4B), laterally positioned tubercles on metatarsals II and III, metatarsal II wider proximally than metatarsal III, and the ligament pits of metatarsal I being present on the lateral surface only. Taking that into account, I consider ZPAL MgD-I/97 to belong to the same species as MPC-D 100/980, collected from the same site and strata. Hence, I suggest that some slight differences mentioned in the description in the anatomy of the particular bones between the specimens are most likely explainable by individual variation.

The phylogenetic analyses of Turner et al. (2021) and Napoli et al. (2021) recovered the holotype of *S. devi* as a sister to *V. mongoliensis*. New data from the specimen ZPAL MgD-I/97 support these results, recovering closely related *S. devi* and *V. mongoliensis* within Velociraptorinae, the result obtained also from the dataset modified from Powers et al. (2022; Fig. 6). Addition of new data on *S. devi* does not change the overall topologies of the trees and only slightly changes the support for the clades within Eudromaeosauria, which remains low (Bootstrap values below 70). The only major change in results from Napoli et al. (2021) is recovering *Shanag* as a member of Saurornitholestinae, together with *Bambiraptor* and *Saurornitholestes*, and the group forming a clade with Velociraptorinae rather than Dromaeosaurinae. In the recent analyses of Wang et al. (2022), the holotype of *S. devi*, *K. kulla*, and *Adasaurus mongoliensis* were recovered as belonging to the clade containing *Atrociraptor marshalli* and *Saurornitholestes langstoni*. ZPAL MgD-I/97 reveals that *S. devi* shares crucial cranial features with *V. mongoliensis*, among all, the position and morphology of the maxillary and promaxillary fenestrae, and the low maxilla below the antorbital fossa. The differences in skulls of *S. devi* and *V. mongoliensis* do not exceed the variation expected for the single genus. Although *S. devi* shares some cranial features (the Z-shaped maxillo-jugal suture and the posterior placement of the last maxillary tooth) with both *Atrociraptor* and *Saurornitholestes*, they are likely convergences caused by the development of a relatively short skull rather than evidence of close affinities with the North American taxa.

Fig. 9. Artistic post-mortem reconstruction of the *Shri devi* Turner, Montanari, and Norell, 2021, individual represented by a specimen ZPAL MgD-I/97 before its final burial. Artwork by Jakub Zalewski (CC BY-NC-ND-3.0).

It was suggested that the sample of *V. mongoliensis* known from the Djadokhta strata may represent more than one species (Powers et al. 2020, 2022). *Velociraptor* sp. (MPC-D 100/982) from Bayan Zag was recovered as significantly distinct in maxillary morphology from the other specimens of *V. mongoliensis* (Powers et al. 2022; Fig. 5A). However, the only velociraptorine specimen from the same site that includes cranial material is the holotype of *V. mongoliensis*, AMNH FARB 6515, and the PCA recover them close to each other along the PC1 axis, although being widely separated along the PC2. The two skulls are both quite dorsoventrally low in overall morphology, and the subtle labial ridge of the maxilla seems to extend posteriorly onto the lateral surface of the jugal. Specimens from Tögrögiin Shiree have generally dorsoventrally higher skulls in lateral view, with less constriction of the skull within the maxillo-jugal contact (Fig. 7). As was observed on specimens of the protoceratopsid *Protoceratops andrewsi*, there is some degree of intraspecific variation within the samples collected from the Bayan Zag and Tögrögiin Shiree sites (Czepiński 2020b). It was suggested as possible evidence for differences in the geological age of the strata of both sites or some regional radiation (Czepiński 2020a; for discussion on stratigraphy controversy see: Dashzeveg et al. 2005; Hasegawa et al. 2009; Jerzykiewicz et al. 2021). Such variation between samples from the particular Djadokhta sites would be expected also in other vertebrates known from the high number of specimens. Regarding that in the past morphology of the particular elements for *V. mongoliensis* was described on the basis of specimens that are no longer referable to that species, e.g. the palate region described by Barsbold and Osmólska (1999) based on ZPAL MgD-I/97, there is a need of the redescription of *V. mongoliensis* on the basis of the well-preserved, and highly diagnostic specimens, with further discussion on possible differences between the material collected from different sites.

Within dromaeosaurids, the elongated snouts are present only in velociraptorines from the Gobi Basin. However, the skull of *S. devi* is relatively short anteroposteriorly and high dorsoventrally when compared to other members of Velociraptorinae (the estimated length to height ratio of maxilla is in range of 1.90–2.25 for ZPAL MgD-I/97, while being in range from 2.42 in *Linheraptor exquisitus* to 3.39 in *Velociraptor* sp. [MPC-D 100/982]), more comparable to the range of variation within *Saurornitholestes langstoni* (Fig. 6). The preserved portion of the skull suggests that the whole cranium of *S. devi* (ZPAL MgD-I/97) was relatively large, only slightly smaller than *V. mongoliensis* (MPC-D 100/25) and *L. exquisitus* (IVVP V16923) (Fig. 7). Hence, most likely the short-faced morphology of ZPAL MgD-I/97 cannot be explained solely by the ontogeny of these other taxa.

As observed by Powers et al. (2020, 2022), the elongation of the dromaeosaurid snout was related with the depositional environment, with velociraptorines from the aeolian strata of the Gobi Desert having the most elongated snouts, and the other dromaeosaurids from alluvial sediments usually having a lower ratio of the length to height of the maxilla (Fig. 6; Powers et al. 2022). It was interpreted as most likely related to the acquiring of the small-sized prey abundant in the aeolian environment. The Baruungoyot strata, yielding the *S. devi* material (Fig. 9), was reported to record the intermediate environment between the aeolian Djadokhta (together with Bayan Mandahu and Ukhaa Tolgod) and the fluvial Nemegt strata (Jerzykiewicz et al. 1993; 2021). However, the overall vertebrate fauna composition is not significantly different between the Djadokhta and Baruungoyot sites, both being dominated by small and medium-sized animals (lizards, mammals, protoceratopsids, oviraptorosaurs, and birds) with rare larger ankylosaurids (Czepiński 2020a; Jerzykiewicz et al. 2021), suggesting the similar size of the prey in both environments. The skull of *S. devi*, although short, was still rather slender, in contrast to the more robust morphology observed in *Achillobator giganticus*, *Atrociraptor marshalli*, *Deinonychus antirrhopus*, and *Dromaeosaurus albertensis*. Alternatively, it was suggested that the elongation of the snout in dromaeosaurids may be a result of the expansion of the pneumatic sinuses (Witmer 1997), potentially related with thermoregulation, hence the animals living in the more arid environment would tend to elongate the maxilla (Powers et al. 2020). Given the presence of the two coeval velociraptorines in the Khulsan site, *S. devi* and *K. kulla*, it is possible that a niche partitioning between them resulted in shortening of the snout of one species; however, more complete cranial material of both taxa is essential for testing this hypothesis.

Acknowledgements

I am grateful to Mateusz Tałanda and Jerzy Dzik (both University of Warsaw, Poland), Philip Currie and Mark Powers (both UALVP), Andrew Farke (Raymond M. Alf Museum of Paleontology, Claremont, USA), and Daniel Madzia (ZPAL) for their helpful suggestions and discussions that greatly improved my manuscript. I thank David Hone (Queen Mary University of London, UK), and Alan Turner and James Napoli (both AMNH) for providing photographs and measurements of dromaeosaurid specimens that were not available for my first-hand examination. I also thank Daniel Barta (Oklahoma State University, Tahlequah, USA) for the editorial care. I thank Szymon Łukasiewicz (Military University of Technology, Warsaw, Poland) for production of the CT scans, Tomasz Szczygielski (ZPAL) for help with the surface scanning, Jolanta Kobylińska (ZPAL) for help with access to the specimen and obtaining the archival photographs from the Polish-Mongolian Paleontological Expeditions, Boban Filipović (Užice, Serbia) and Maciej Ziegler (Poznań, Poland) for sharing their observations, and Jakub Zalewski (University of Warsaw, Poland) for creating the artwork on the Fig. 9. This project was supported by the National Science Centre, Poland, grant no. 2020/36/T/NZ8/00395.

References

Barsbold, R. 1983. Carnivorous dinosaurs from the Cretaceous of Mongolia [in Russian]. *Sovmestnaâ Sovetsko-Mongol'skaâ Paleontologičeskaâ Ekspeditciâ, Trudy* 19: 1–117.

Barsbold, R. and Osmólska, H. 1999. The skull of *Velociraptor* (Theropoda) from the Late Cretaceous of Mongolia. *Acta Palaeontologica Polonica* 44: 189–219.

Benton, M.J. 2000. Conventions in Russian and Mongolian palaeontological literature. *In*: M.J. Benton, M.A. Shishkin, D.M. Unwin, and E.N. Kurochkin (eds.), *The Age of Dinosaurs in Russia and Mongolia*, xxii–xxviii. Cambridge University Press, Cambridge.

Brownstein, C.D. 2021. Dromaeosaurid crania demonstrate the progressive loss of facial pneumaticity in coelurosaurian dinosaurs. *Zoological Journal of the Linnean Society* 191: 87–112.

Burnham, D.A., Derstler, K.L., Currie, P.J., Bakker, R.T., Zhou, Z., and Ostrom, J.H. 2000. Remarkable new birdlike dinosaur (Theropoda: Maniraptora) from the Upper Cretaceous of Montana. *The University of Kansas Paleontological Contributions* 13: 1–14.

Cau, A. and Madzia, D. 2018. Redescription and affinities of *Hulsanpes perlei* (Dinosauria, Theropoda) from the Upper Cretaceous of Mongolia. *PeerJ* 6: e4868.

Cau, A., Beyrand, V., Voeten, D.F., Fernandez, V., Tafforeau, P., Stein, K., Barsbold, R., Tsogtbaatar, K., Currie, P.J., and Godefroit, P. 2017. Synchrotron scanning reveals amphibious ecomorphology in a new clade of bird-like dinosaurs. *Nature* 552: 395–399.

Chen, X., Tan, K., Lu, L., and Ji, S.A. 2022. Occurrence of *Protoceratops hellenikorhinus* (Ceratopsia: Protoceratopsidae) in Alxa region, western Inner Mongolia, China. *Acta Geologica Sinica* 96: 3722–3732.

Cignoni, P., Callieri, M., Corsini, M., Dellepiane, M., Ganovelli, F., and Ranzuglia, G. 2008. Meshlab: an open-source mesh processing tool. *In*: *Sixth Eurographics Italian Chapter Conference*, 129–136.

Currie, P.J. and Evans, D.C. 2020. Cranial anatomy of new specimens of *Saurornitholestes langstoni* (Dinosauria, Theropoda, Dromaeosauridae) from the Dinosaur Park Formation (Campanian) of Alberta. *The Anatomical Record* 303: 691–715.

Currie, P.J. and Varricchio, D.J. 2004. A new dromaeosaurid from the Horseshoe Canyon Formation (Upper Cretaceous) of Alberta, Canada. *In*: P.J. Currie, E.B. Koppelhus, M.A. Shugar, and J.L. Wright (eds.), *Feathered Dragons: Studies on the Transition from Dinosaurs to Birds*, 112–132, Indiana University Press, Bloomington.

Czepiński Ł. 2020a. New protoceratopsid specimens improve the age correlation of the Upper Cretaceous Gobi Desert strata. *Acta Palaeontologica Polonica* 65: 481–497.

Czepiński, Ł. 2020b. Ontogeny and variation of a protoceratopsid dinosaur *Bagaceratops rozhdestvenskyi* from the Late Cretaceous of the Gobi Desert. *Historical Biology* 32: 1394–1421.

Dashzeveg, D., Dingus, L., Loope, D.B., Swisher, C.C., Dulam, T., and Sweeney, M.R. 2005. New stratigraphic subdivision, depositional environment, and age estimate for the Upper Cretaceous Djadokhta Formation, southern Ulan Nur Basin, Mongolia. *American Museum Novitates* 3498: 1–31.

Dingus, L., Loope, D.B., Dashzeveg, D., Swisher, C.C., Minjin, C., Novacek, M.J., and Norell, M.A. 2008. The geology of Ukhaa Tolgod (Djadokhta Formation, Upper Cretaceous, Nemegt Basin, Mongolia). *American Museum Novitates* 2008: 1–40.

Evans, D.C., Larson, D.W., and Currie, P.J. 2013. A new dromaeosaurid (Dinosauria: Theropoda) with Asian affinities from the latest Cretaceous of North America. *Naturwissenschaften* 100: 1041–1049.

Feduccia, A., Martin, L.D., and Tarsitano, S. 2007. Perspectives in Ornithology *Archaeopteryx* 2007: Quo Vadis? *The Auk* 124: 373–380.

Godefroit, P., Currie, P.J., Hong, L., Yong, S.C., and Dong, Z. 2008. A new species of *Velociraptor* (Dinosauria: Dromaeosauridae) from the Upper Cretaceous of northern China. *Journal of Vertebrate Paleontology* 28: 432–438.

Goloboff, P.A. and Morales, M.E. 2023. TNT version 1.6, with a graphical interface for MacOS and Linux, including new routines in parallel. *Cladistics* 39: 1–10.

Hammer, Ø., Harper, D.A., and Ryan, P.D. 2001. PAST: Paleontological statistics software package for education and data analysis. *Palaeontologia Electronica* 4: 1–9.

Hasegawa, H., Tada, R., Ichinnorov, N., and Minjin, C. 2009. Lithostratigraphy and depositional environments of the Upper Cretaceous Djadokhta Formation, Ulan Nuur basin, southern Mongolia, and its paleoclimatic implication. *Journal of Asian Earth Sciences* 35: 13–26.

Hattori, S. 2016. Evolution of the hallux in non-avian theropod dinosaurs. *Journal of Vertebrate Paleontology* 36: e1116995.

Hendrickx, C., Mateus, O., and Araújo, R. 2015. A proposed terminology of theropod teeth (Dinosauria, Saurischia). *Journal of Vertebrate Paleontology* 35: e982797.

Hone, D., Tsuihiji, T., Watabe, M., and Tsogtbaatar, K. 2012. Pterosaurs as a food source for small dromaeosaurs. *Palaeogeography, Palaeoclimatology, Palaeoecology* 331: 27–30.

Jerzykiewicz, T. and Russell, D.A. 1991. Late Mesozoic stratigraphy and vertebrates of the Gobi Basin. *Cretaceous Research* 12: 345–377.

Jerzykiewicz, T., Currie, P.J., Eberth, D.A., Johnston, P.A., Koster, E.H., and Zheng, J.J. 1993. Djadokhta Formation correlative strata in Chinese Inner Mongolia: an overview of the stratigraphy, sedimentary geology, and paleontology and comparisons with the type locality in the pre-Altai Gobi. *Canadian Journal of Earth Sciences* 30: 2180–2195.

Jerzykiewicz, T., Currie, P.J., Fanti, F., and Lefeld, J. 2021. Lithobiotopes of the Nemegt Gobi Basin. *Canadian Journal of Earth Sciences* 58: 829–851.

Kirkland, J.I., Burge, D., and Gaston, R. 1993. A large dromaeosaur (Theropoda) from the Lower Cretaceous of eastern Utah. *Hunteria* 2: 1–16.

Lee, S., Lee, Y.N., Currie, P.J., Sissons, R., Park, J.Y., Kim, S.H., Barsbold, R., and Tsogtbaatar, K. 2022. A non-avian dinosaur with a streamlined body exhibits potential adaptations for swimming. *Communications Biology* 5: 19.

Limaye, A. 2012. Drishti: a volume exploration and presentation tool. *Developments in X-ray Tomography VIII, Proceedings Volume* 8506: 191–199.

Marsh, O.C. 1881. Principal characters of American Jurassic dinosaurs, part V. *American Journal of Science* 3: 417–423.

Matthew, W.D. and Brown, B. 1922. The family Deinodontidae, with notice of a new genus from the Cretaceous of Alberta. *Bulletin of the American Museum of Natural History* 46: 367–385.

Napoli, J.G., Ruebenstahl, A.A., Bhullar, B.A.S., Turner, A.H., and Norell, M.A. 2021. A new dromaeosaurid (Dinosauria: Coelurosauria) from Khulsan, central Mongolia. *American Museum Novitates* 3892: 1–47.

Norell, M.A. and Makovicky, P.J. 1997. Important features of the dromaeosaur skeleton: information from a new specimen. *American Museum Novitates* 3215: 1–28.

Norell, M.A. and Makovicky, P.J. 1999. Important features of the dromaeosaurid skeleton II: Information from newly collected specimens of *Velociraptor mongoliensis*. *American Museum Novitates* 3282: 1–45.

Norell, M.A., Clark, J.M., Turner, A.H., Makovicky, P.J., Barsbold, R., and Rowe, T. 2006. A new dromaeosaurid theropod from Ukhaa Tolgod (Ömnögov, Mongolia). *American Museum Novitates* 3545: 1–51.

Norell, M.A., Makovicky, P.J., and Clark, J.M. 2004. The braincase of *Velociraptor*. *In*: P.J. Currie, E.B. Koppelhus, M.A. Shugar, and J.L. Wright (eds.), *Feathered Dragons: Studies on the Transition from Dinosaurs to Birds*, 133–143. Indiana University Press, Bloomington.

Osborn, H.F. 1924. Three new Theropoda, *Protoceratops* zone, Central Mongolia. *American Museum Novitates* 144: 1–12.

Osmólska, H. 1981. Coossified tarsometatarsi in theropod dinosaurs and their bearing on the problem of bird origins. *Palaeontologia Polonica* 42: 79–95.

Osmólska, H. 1982. *Hulsanpes perlei* n.g. n.sp. (Deinonychosauria, Saurischia, Dinosauria) from the Upper Cretaceous Barun Goyot Formation of Mongolia. *Neues Jahrbuch für Geologie und Paläontologie Monatshefte* 1982: 440–448.

Ostrom, J.H. 1969. Osteology of *Deinonychus antirrhopus*, an unusual theropod from the Lower Cretaceous of Montana. *Peabody Museum of Natural History Bulletin* 30: 1–165.

Owen, R. 1842. Report on British fossil reptiles, part II. *Report for the British Association for the Advancement of Science, Plymouth* 1841: 60–294.

Pittman, M., O'Connor, J., Field, D.J., Turner, A.H, Ma, W., Makovicky, P., and Xu, X. 2020a. Pennaraptoran systematics. *Bulletin of the American Museum of Natural History* 440: 7−36.

Pittman, M., O'Connor, J., Tse, E., Makovicky, P., Field, D.J., Ma, W., Turner, A.H., Norell, M.A., Pei, R., and Xu, X. 2020b. The fossil record of Mesozoic and Paleocene pennaraptorans. *Bulletin of the American Museum of Natural History* 440: 37−95.

Powers, M.J., Fabbri, M., Doschak, M.R., Bhullar, B.A.S., Evans, D.C., Norell, M.A., and Currie, P.J. 2022. A new hypothesis of eudromaeosaurian evolution: CT scans assist in testing and constructing morphological characters. *Journal of Vertebrate Paleontology* 41: e2010087.

Powers, M.J., Sullivan, C., and Currie, P.J. 2020. Re-examining ratio based premaxillary and maxillary characters in Eudromaeosauria (Dinosauria: Theropoda): Divergent trends in snout morphology between Asian and North American taxa. *Palaeogeography, Palaeoclimatology, Palaeoecology* 547: 109704.

Schindelin, J., Arganda-Carreras, I., Frise, E., Kaynig, V., Longair, M., Pietzsch, T., Preibisch, S., Rueden, C., Saalfeld, S., Schmid, B., Tinevez, J.Y., White, D.J., Hartenstein, V., Eliceiri, K., Tomancak, P., and Cardona, A. 2012. Fiji: an open-source platform for biological-image analysis. *Nature Methods* 9: 676–682.

Semple, T.L., Peakall, R., and Tatarnic, N.J. 2019. A comprehensive and user-friendly framework for 3D-data visualisation in invertebrates and other organisms. *Journal of Morphology* 280: 223–231.

Sues, H.D. 1977. The skull of *Velociraptor mongoliensis*, a small Cretaceous theropod dinosaur from Mongolia. *Paläontologische Zeitschrift* 51: 173–184.

Tsogtbaatar, K., Weishampel, D.B., Evans, D.C., and Watabe, M. 2019. A new hadrosauroid (Dinosauria: Ornithopoda) from the Late Cretaceous Baynshire Formation of the Gobi Desert (Mongolia). *PLoS One* 14: e0208480.

Turner, A.H., Makovicky, P.J., and Norell, M.A. 2012. A review of dromaeosaurid systematics and paravian phylogeny. *Bulletin of the American Museum of Natural History* 371: 1–206.

Turner, A.H., Montanari, S., and Norell, M.A. 2021. A new dromaeosaurid from the Late Cretaceous Khulsan Locality of Mongolia. *American Museum Novitates* 3965: 1–48.

Turner, A.H., Pol, D., Clarke, J.A., Erickson, G.M., and Norell, M.A. 2007. A basal dromaeosaurid and size evolution preceding avian flight. *Science* 317: 1378–1381.

Wang, X., Cau, A., Guo, B., Ma, F., Qing, G., and Liu, Y. 2022. Intestinal preservation in a birdlike dinosaur supports conservatism in digestive canal evolution among theropods. *Scientific Reports* 12: 1–10.

Watabe, M., Tsogtbaatar, K., Suzuki, S., and Saneyoshi, M. 2010. Geology of dinosaur-fossil-bearing localities (Jurassic and Cretaceous: Mesozoic) in the Gobi Desert: Results of the HMNS-MPC Joint Paleontological Expedition. *Hayashibara Museum of Natural Sciences Research Bulletin* 3: 41–118.

Witmer, L.M. 1997. The evolution of the antorbital cavity of archosaurs: a study in soft-tissue reconstruction in the fossil record with an analysis of the function of pneumaticity. *Journal of Vertebrate Paleontology* 17: 1–76.

Xu, X. and Wu, X.C. 2001. Cranial morphology of *Sinornithosaurus millenii* Xu et al. 1999 (Dinosauria: Theropoda: Dromaeosauridae) from the Yixian formation of Liaoning, China. *Canadian Journal of Earth Sciences* 38: 1739–1752.

Xu, X., Choiniere, J.N., Pittman, M., Tan, Q., Xiao, D., Li, Z., Tan, L., Clark, J.M., Norell, M.A., Hone, D., and Sullivan, C. 2010. A new dromaeosaurid (Dinosauria: Theropoda) from the Upper Cretaceous Wulansuhai Formation of Inner Mongolia, China. *Zootaxa* 2403: 1–9.

Xu, X., Pittman, M., Sullivan, C., Choiniere, J.N., Tan, Q.W., Clark, J.M., Norell, M.A., and Shuo, W. 2015. The taxonomic status of the Late Cretaceous dromaeosaurid *Linheraptor exquisitus* and its implications for dromaeosaurid systematics. *Vertebrata PalAsiatica* 53: 29–62.